Computer-Assisted Diagnosis of Cardiac Perfusion Studies

Frank V. Gabor, Frederick L. Datz, Paul E. Christian, Grant T. Gullberg, and Kathryn A. Morton

University of Utah Medical Center, Salt Lake City, Utah

Quantitative analysis of nuclear medicine images is becoming increasingly widespread. In addition to thallium myocardial studies, regional quantitation programs exist for ventriculography and cerebral perfusion studies. Computer-assisted diagnosis is being developed for other areas as well, such as lung scintigraphy (*1*).

Interest in computer-aided-diagnosis of nuclear medicine images exists because of a need to standardize and objectively analyze studies, eliminating inter-observer variations in interpretation. The goal of quantitation is to be able to approximate, and in some cases, improve on the results of visual interpretation. Published results indicate variable success. For example, the sensitivity rate for determining coronary artery disease in thallium studies by quantitation has been as high as 95% (*2*).

Quantitative methods usually involve comparison of count densities in a specific area to that of a normal file, or to another region of the scan in which the activity is thought to be independent of the disease process. Problems can occur in quantitation when variations exist in the size and shape of the subject and organ in question. Without accurate body contour detection, this will cause improper attenuation correction and thus may prevent accurate computer analysis.

POLAR PLOT

The bull's eye or polar plot maps three-dimensional cardiac data from a single-photon emission computed tomography (SPECT) acquisition. This allows the visualization of all the tomographic slices in one plane as a single image. The short-axis slices are used since they include all myocardial walls. The polar plot can be created with either exercise or pharmacologic thallium studies, although normal databases are currently valid only with exercise studies (*3*). The horizontal long-axis slice with the greatest cavity is used as a guide for selection of the short-axis slices to be used. Short-axis slices of equal thickness are produced from the apex to the base; the total number of slices obtained is standardized per system and is usually fifteen.

For reprints contact: Frederick L Datz, MD, Nuclear Medicine Division, University of Utah Medical Center, Salt Lake City, Utah 84132.

After the center of the left ventricle is identified, each slice is subtended into 40 nine-degree sectors with maximal counts per sector determined. The maximal counts per sector are then plotted circumferentially in concentric rings, starting with the apex in the center and proceeding peripherally to the base. Special concern is given to the apex. Due to apical thinning and the effects of partial volume averaging, each of the two slices nearest the apex is usually represented as a single value rather than as forty separate counts.

Because the polar plot is still a representation of the heart along the transaxial plane, the orientation of the myocardial walls remains the same, with the septum on the left, lateral wall on the right, the anterior wall superiorly, and the inferoposterior wall at the bottom on the plot (*2,4*) (Fig. 1).

Both stress and delayed images can be displayed in this format. In order to obtain comparable images, the delayed polar plot may subsequently be normalized to the stress plot based on the maximum count per pixel from both stress and redistribution images. A percent washout plot may also be calculated using the stress and non-normalized redistribution images. Since plots are standardized, pixel by pixel comparison of the delayed and stress plots ensures comparison of like areas. The display uses either a gray scale or color code (Fig. 2).

To determine abnormal regions, the count profiles for stress and redistribution are compared to a file of normals. A level of 2.5 s.d. below normal is used as the threshold for flagging defects (*2*). This limit has been shown to offer the best compromise between sensitivity and specificity. Optimally, comparison should be made with gender-matched normals. The gender-matched normal files are obtained from a group of patients with a low likelihood of coronary artery disease (*3,5–7*).

To prevent noise or statistical aberration from causing a false-positive scan, abnormal pixels are subjected to a clustering criterion whereby two adjacent neighbors must also be abnormal in order to display the original pixel as abnormal. The comparison map obtained is usually displayed with defects blacked out and other points displayed via a color map or gray scale based on the number of s.d. from normal.

Recently, an additional polar plot has been developed to distinguish fixed defects from reversible ones (infarct versus

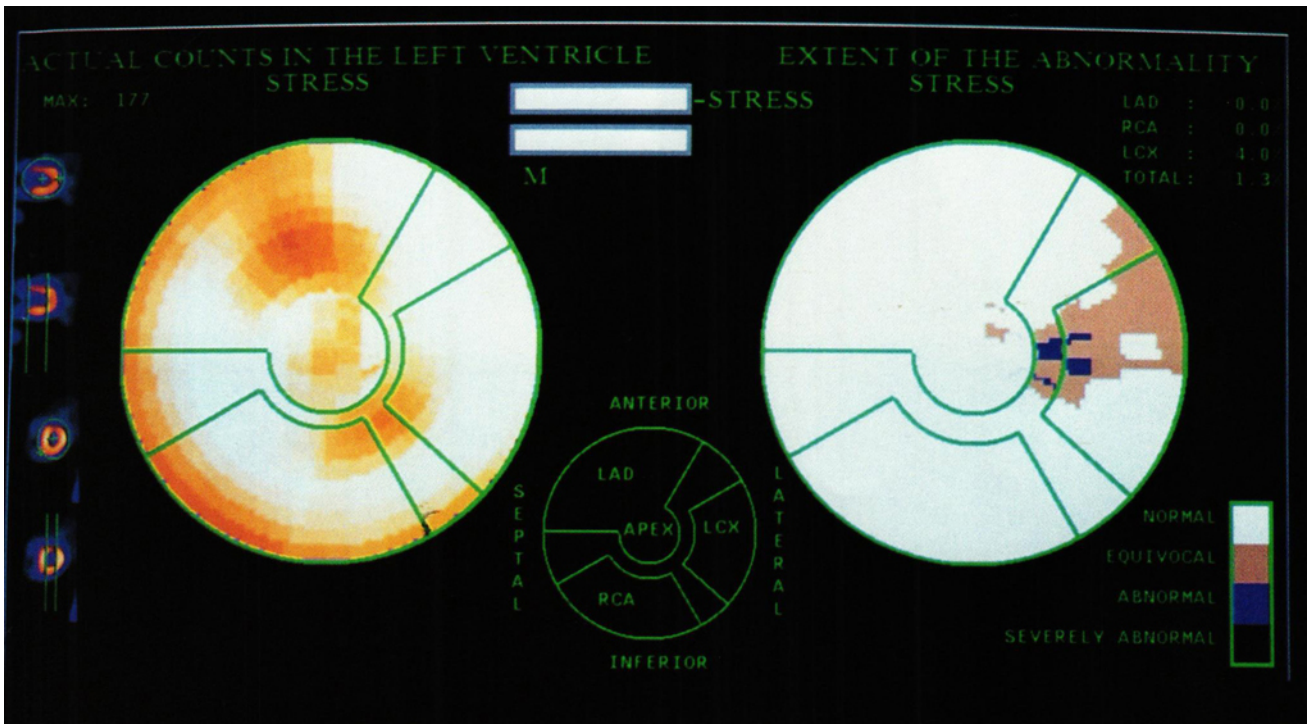

FIG. 1. Normal polar plot.

ischemia) (*8*). Called a reversibility plot, it is created by subtracting each point in the patient's normalized stress plot from the normalized redistribution plot. Areas which do not redistribute are displayed as black with reversible regions displayed as blue to white depending on the degree of reversibility. Again, this depends on how far the points fall from a gender-matched normal file, measured in s.d.

Although early reports indicated sensitivities of up to 95% (*2*) for detecting coronary artery disease (defined as a coronary artery stenosis greater than 50%), more recent studies indicate sensitivities of 73% for reversible defects and 80% for fixed defects (*9*). Reported specificities for coronary artery disease detection have ranged from 44% to 74% (*2,10*). The low specificity rate may be due in part to post-test referral bias. Patients with positive thallium-201 (^{201}Tl) scintigrams will preferentially be selected for cardiac catheterization, resulting in a skewed population; this will falsely decrease the specificity.

Due to the importance of determining which coronary arteries are diseased, an attempt has been made to associate defects determined by quantitative means with specific coronary vessels. This is done by dividing the polar maps into regions of interest and associating them with vessels known to supply those areas. The left anterior descending artery is known to supply the antero-septum and thus defects in this region (left and superior portion of the plot) are attributed to disease of this artery. Likewise, the left circumflex artery supplies the lateral wall and the right coronary artery supplies the infero-septum. Unfortunately, because of inter-patient variation and significant overlap of vascular territory, it is not possible to clearly demarcate regions of supply. Sensitivities for quantitatively determined specific coronary artery involvement reflect this problem with the worst localization seen in left circumflex lesions and the best in right coronary artery lesions. However, the literature shows that quantitative determination of diseased vessels compares favorably with visual determination (*2*) (Fig. 3).

Sources of Error

Several factors can influence the accuracy of quantitative cardiac analysis. Sources of error include those caused by normal variants, gender differences, and imaging artifacts.

The apex of the heart is especially prone to artifacts. Since determination of the short-axis tomographic slice nearest the apex is operator dependent, a misplaced apical slice may not truly reflect actual apical counts. An apical slice with a significant portion of background within the slice may have a decreased count density due to partial volume averaging. Additionally, decreased counts can be the result of normal apical thinning. Some systems attempt to overcome this by using the maximum count per pixel within the entire apical slice to represent the entire apex (*2*). Other systems try to eliminate operator dependence in choosing the slice nearest the apex by using the vertical long axis to obtain count information about the apex (*11*). Occasionally, apical thinning will be displaced laterally or, less frequently, septally. This can potentially create an artifactual defect (*7*). Visual inspection of the horizontal long-axis slices can alert the operator to this possibility.

Myocardial hot spots, frequently attributed to papillary muscle insertion, can also cause artifacts (*7*). Since polar plots are normalized to the area of greatest myocardial count

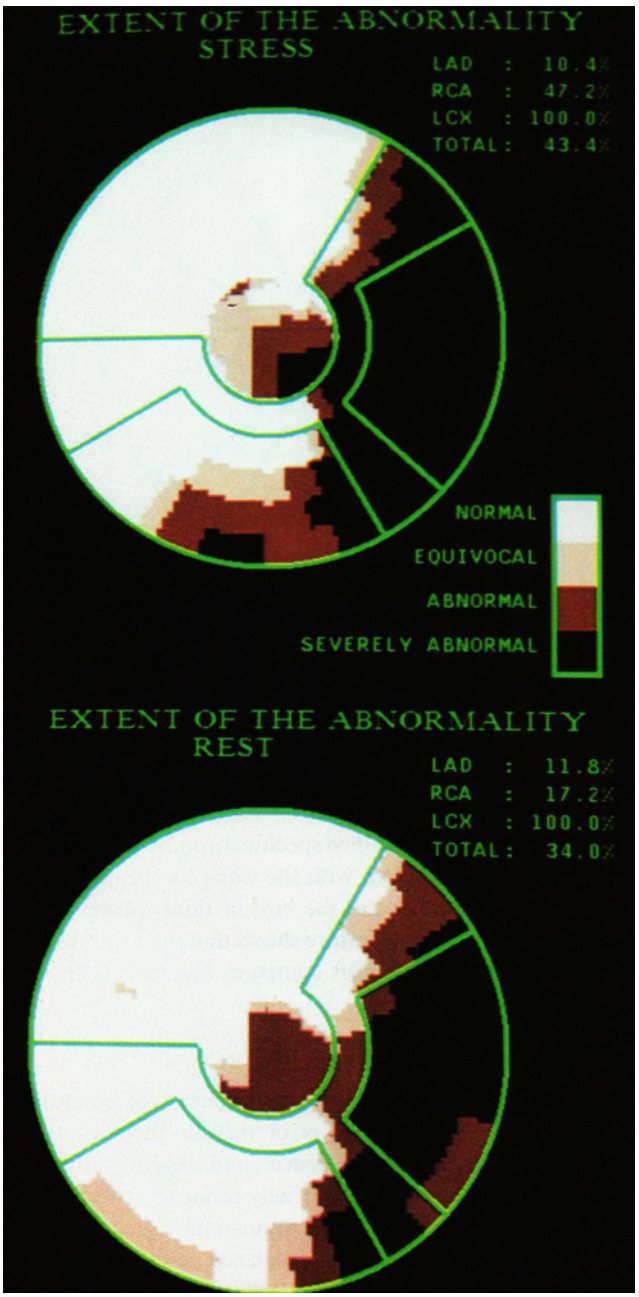

FIG. 2. Polar plot showing a large inferolateral defect on the stress image. The lateral defect remains on rest although the inferior defect does redistribute indicating lateral infarct with inferior ischemia.

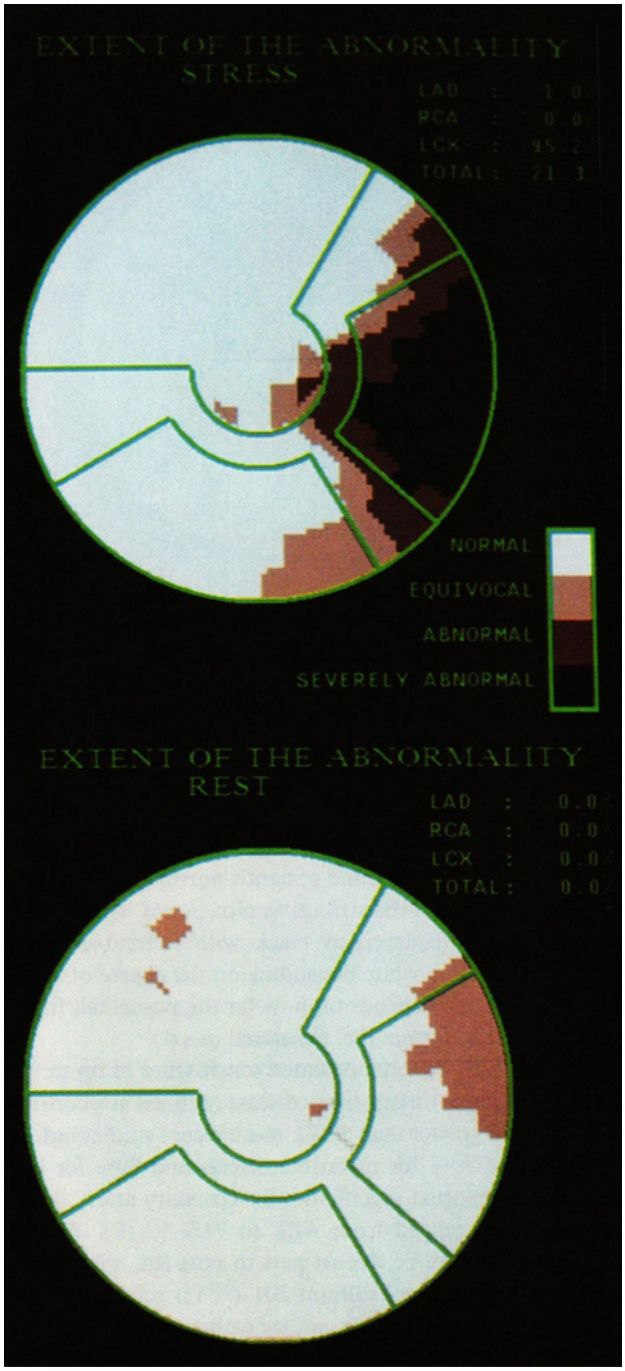

FIG. 3. Polar plot demonstrating a large defect on stress in the distribution of the left circumflex artery, which redistributes on rest indicating lateral ischemia.

density, hot spots can cause the remainder of the myocardium to appear to have a diminished count density; this will produce a false-positive scan. Again, correlation with the tomographic slices is important in order to recognize this problem.

Variations in relative count density can also occur due to various physiologic conditions. Left bundle branch block has been shown to produce septal defects in patients with angiographically proven normal coronary arteries (*7*). Left ventricular hypertrophy can cause a relative decrease in lateral wall counts, which may mimic a defect in this region (*7*). Thus, it is imperative to obtain the patient's history before interpreting these studies.

Gender differences must also be taken into consideration. There are relative differences in average count densities in the myocardial walls in both males and females.The lateral wall generally has the greatest count density, while the septum has the least. The principle difference in regional uptake between normal men and women is decreased anterior and upper

septal count densities in women. This is reflected in an anterior to inferior count ratio in men of approximately 1:2; in women this ratio is closer to 1 (*5,6*). This difference is due to anterior wall attenuation by overlying breast tissue in women (Fig. 4). Additionally, there is relatively decreased count density in the inferior walls of males, presumably due to diaphragmatic attenuation.

These variations emphasize the need for normal files to be gender-matched. However, consideration must be given to the body habitus of each patient, as well. For example, male patients with gynecomastia will exhibit anterior wall attenuation similar to women, whereas thallium studies on women who have undergone left mastectomies are more likely to resemble those of males.

There are technical factors which can also create imaging artifacts. While slight patient motion is tolerable and does not appear to interfere with the study, motion significant enough to produce imaging artifacts occurs in up to 10% of quantitative studies. Motion will be manifested on polar plots as defects whose location is dependent on the direction of the patient motion.

Several investigators have attempted to develop motion detection and correction algorithms. A cross-correlation algorithm has been created to detect sudden motion in the vertical direction (*12*). Frame-to-frame pixel shift that deviates beyond an established threshold from a parabolically fit distribution profile is assumed to be motion and is shifted. Alternatively, a diverging squares algorithm has been devised that attempts to track the center of the left ventricle and detect motion in two directions (*13*). This is done by expanding a box placed interactively in the left ventricle in the direction of maximal counts. If motion detection algorithms are to be successful, they must detect motion in all planes, detect both abrupt and gradual motion, and work both with stress and redistribution images. Currently, employment of these algorithms is often unsuccessful (Fig. 5).

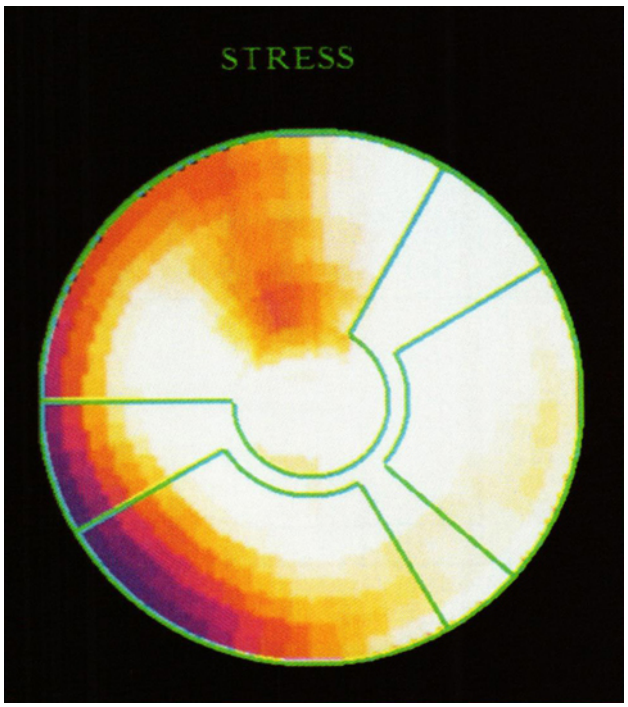

FIG. 4. Anterior wall defect due to breast attenuation.

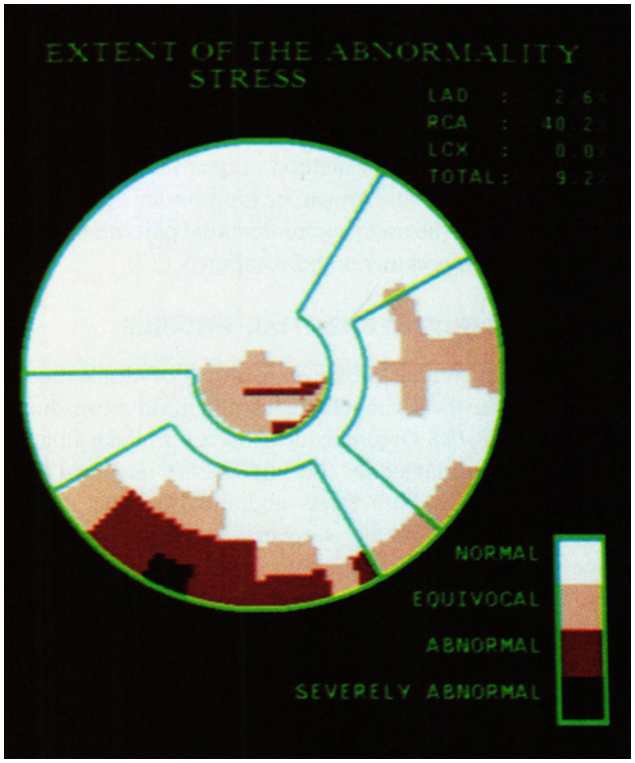

FIG. 5. Large inferior wall defect due to patient motion.

An additional source of motion is heart creep, the phenomenon of upward movement of the heart immediately after exercise (*14*). This upward motion is most likely due to transient increase of mean total lung volume following exercise. The result is an inferiorly displaced heart, which subsequently returns to baseline. This movement tends to produce antero-septal and infero-septal ischemia on imaging. Waiting approximately 15 min after stress before initiating SPECT acquisition generally avoids this phenomenon (*14,15*). Since this movement is probably due to slow, continuous motion, performing a weighted interpolated shift in the vertical direction should correct the images. A similar phenomenon may also be seen with leg flexion (*16*).

Errors in reconstruction will be reflected in polar plot displays (*7*). For example, distortions can occur if the axis of reconstruction is incorrectly selected and, rather than bisecting the apex, it is somewhat skewed. In this situation, decreased count densities will occur basally in addition to misrepresentation of the apex.

Validation

A multicenter trial was recently undertaken to validate the applicability of quantitative analysis using the polar map display developed at Cedars-Sinai Medical Center (*10*). Var-

ious cameras and computers were used at geographically diverse regions utilizing a gender-matched normal file. Similar sensitivities and specificities were obtained using the multicenter trial population and a prospective population studied at Cedars-Sinai Medical Center. The results indicate the utility of applying the polar plot method of quantitative analysis to a variety of equipment. An earlier multicenter trial had previously validated the use of circumferential plots and washout profiles on various cameras and computers (*17*).

CIRCUMFERENTIAL PROFILE

The circumferential profile is a means of displaying the amount of activity per myocardial segment on a two-dimensional plot (*18,19*). Originally developed for planar imaging, it has also been adapted for use with SPECT imaging (*11*). It can be used with both stress and dipyridamole thallium imaging (*20*). The profile is created by dividing either the planar or tomographic slices into sectors of six degrees and plotting either maximum or average activity in each sector versus sector position for a total of 60 data points. This allows both absolute thallium activity per segment and the relative distribution of activity to be demonstrated. When these profiles are normalized to the segment with the maximum counts and displayed as a percentage of counts versus segment, both stress and delayed images can be displayed on a single graph.

A normal scan should have lines that are nearly superimposed for both studies (Fig. 6), whereas the presence of ischemia will result in a relative increase in counts from stress to redistribution (Fig. 7). Typically, a lower limit of normal is also shown, and segments with counts below this limit that do not improve suggest areas of infarct. The lower limit of normal is calculated to be two s.d. below the mean from a pool of individuals with a low likelihood of coronary artery disease (less than 3%). The integral of the hypoperfused region can also be used as a means to assess the severity of the defect (*20*).

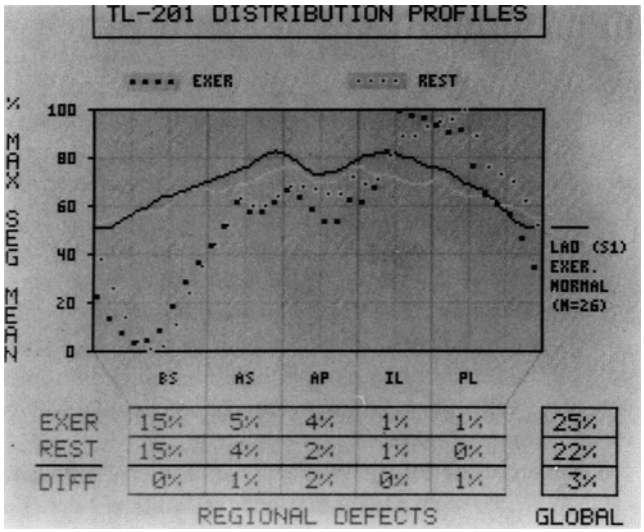

FIG. 7. Abnormal circumferential profile showing decreased counts at both stress and rest in an area of infarct.

WASHOUT PLOT

An additional analytic method originally developed for planar thallium studies is the washout plot (*19*). Thallium washout has been demonstrated to be nearly uniform throughout the myocardium of normal subjects (Fig. 8) but tends to wash out much more slowly from ischemic tissue (*19*). Thallium washout can be displayed graphically by subtracting the non-normalized redistribution circumferential profile from that of stress. Dividing the difference by the stress circumfer-

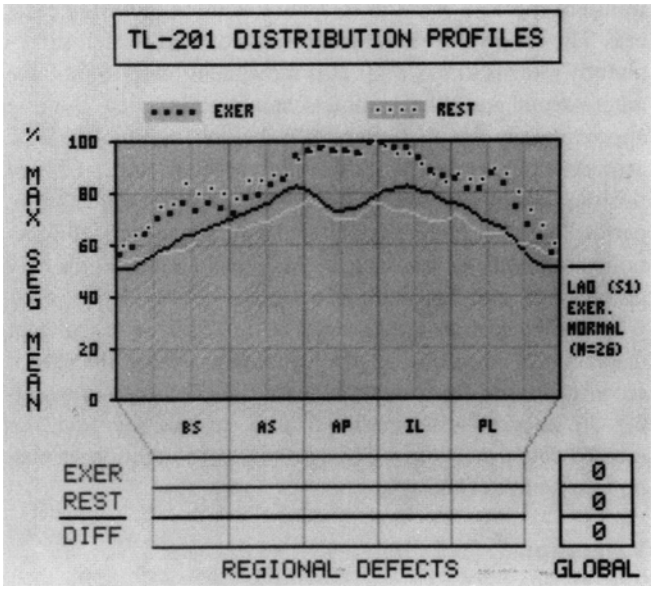

FIG. 6. Normal circumferential profile. Solid black line marks lower limit of normal at stress, while solid white line (nearly superimposed on black line) indicates lower limit of normal at rest.

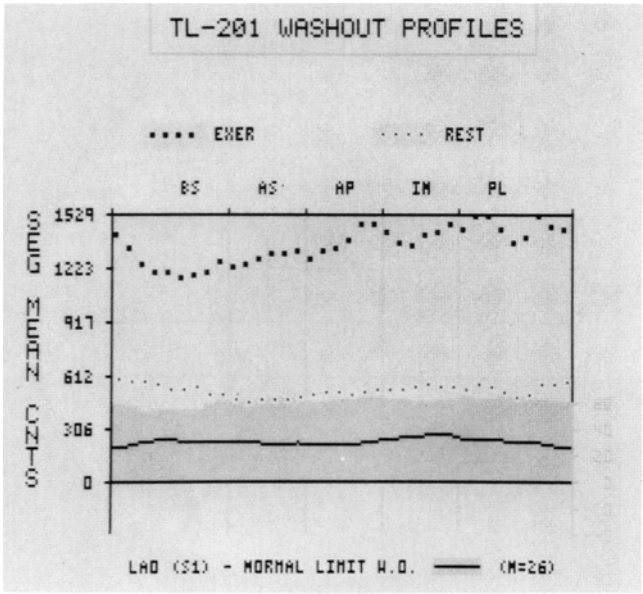

FIG. 8. Normal washout plot. Solid black line indicates lower limit of normal.

ential profile counts yields the percentage of thallium that has washed out of a segment over time. Again, lower limits of normal are established as above, and washout rates that fall two s.d. below normal are flagged as abnormal and indicate ischemia. Infarcted tissue will theoretically have a washout of zero and will also appear abnormal (Fig. 9).

Several technical factors can cause interference with washout curves. The injection site of thallium is important (*21*). Significant residual arm activity occurs in patients when veins other than the medial antecubital vein are used. This results in reduced washout rates, likely due to a slow, constant infusion of thallium into the bloodstream. This may cause an erroneous washout plot that indicates ischemia. Residual arm vein activity has also been associated with injecting thallium in intravenous cannulas that have been in place for over 24 hr (*21*).

Thallium washout appears directly and linearly related to peak heart rate (*22,23*). Slower washouts occur with lower peak heart rates. Thus, patients who achieve a submaximal heart rate response (less than 85% of age-predicted maximum heart rate) may exhibit abnormally delayed washout.

Repositioning changes between stress and redistribution can also contribute to abnormal washout curves (*24*). Errors will generally be manifested in the wall shifted away from the camera.

Variations in the rate of thallium washout have been demonstrated between males and females. Faster washout rates occur in women (*10*). No etiology has yet been suggested for this difference, but it does reinforce the need for gender-matched normals.

Recently, the technique of reinjecting an additional 1 mCi of ^{201}Tl prior to acquiring redistribution images has been advocated (*14,25*). This technique improves the differentiation of viable but ischemic myocardium from areas of infarct.

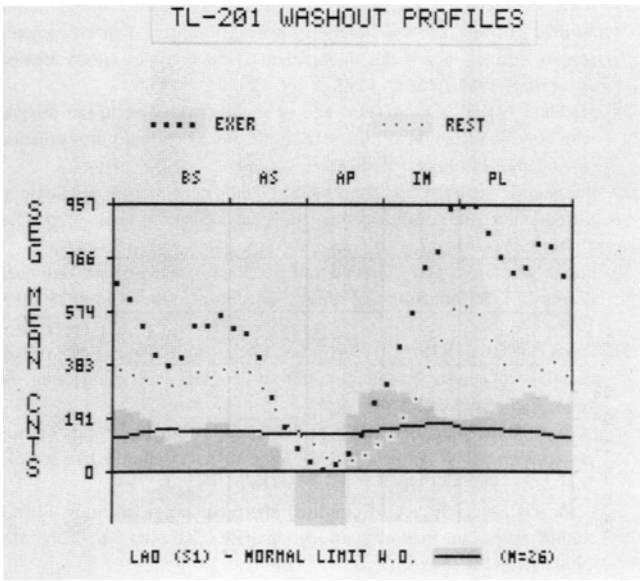

FIG. 9. Abnormal washout demonstrating delayed washout (BS) at an area of ischemia. Absent counts and abnormal washout (AP) are due to infarct.

However, the technique effectively negates any information obtained from washout studies because of the reintroduction of thallium.

Additionally, washout rates in dipyridamole studies have been shown to be slower than with exercise studies (*26*). Since most normal levels are calculated for exercise studies, the washout studies should be ignored in scans using pharmacologic stress unless specific normal files for dipyridamole have been established.

TECHNETIUM AGENTS

Because of thallium's low-energy photon emission and relatively long physical half-life, technetium-labeled myocardial agents have been developed (*14,27*). Technetium-99m (^{99m}Tc) methoxy-isobutyl-isonitrile (sestamibi) compares favorably with ^{201}Tl in detecting coronary artery disease, showing similar sensitivities and specificities. As with thallium studies, quantitative analysis is being developed to aid in the interpretation of ^{99m}Tc sestamibi scans (*27,28*).

Since technetium-99m has a 140-keV photopeak, which is ideal for current imaging systems, image quality tends to be superior to that of ^{201}Tl and less prone to imaging artifacts, such as those produced by soft tissue attenuation (*28*). Thus, myocardium and perfusion defects are better defined. The distribution of ^{99m}Tc sestamibi is similar to that of ^{201}Tl; the lateral wall shows greater activity and the septum shows the least. As with quantitative thallium studies, the need exists for gender-matched normal files.

In a process almost identical to that used for thallium images, a circumferential profile has been developed for ^{99m}Tc sestamibi (*28*). A normal range of count density has been determined for each segment and the lower limit of normal is set at 2.5 s.d. below the mean. Regions falling below this limit are designated as abnormal. Determination of ischemia versus infarct is made on the basis of reversibility of the defect. Since ^{99m}Tc sestamibi studies require injection of the radioisotope at both stress and rest and rest images are generally performed first, washout profiles cannot be obtained. Polar map displays are being developed using the same criteria for detection of coronary artery disease as those used for thallium studies (*27*).

Early analysis of circumferential profiles obtained with ^{99m}Tc sestamibi indicates somewhat improved sensitivity in the quantitative detection of coronary artery disease compared to profiles obtained using ^{201}Tl (*28*). Identification of reversible defects was greater with sestamibi when using a two-day acquisition protocol. Specificities were similar to those obtained with ^{201}Tl. Detection and localization of coronary artery disease using the polar plot method provided similar sensitivities and specificities for ^{201}Tl and ^{99m}Tc sestamibi (*27*).

NEURAL NETWORKS AND EXPERT SYSTEMS

The current methods of myocardial quantitation are all algorithmic-based routines. Another method of computer-aided diagnosis that is non-algorithmic is the neural network

model. Attempts have been made to apply neural networks to radiology (*29,30*). Neural networks differ from conventional artificial intelligence systems in that they do not follow a set of predetermined rules. Rather, they "learn" a task by being trained on a large set of training pairs, which consist of findings and results. This process was applied to interpretation of neonatal chest radiographs with early success (*31*). Although similar neural networks have not yet been developed for interpreting myocardial perfusion defects, some early work has been done in this field (*32,33*). Attempts have also been made to create an expert system by setting up heuristically defined rules that enable the computer to make decisions even in the presence of incomplete data (*8*). Currently, neither method is available for clinical use.

CONCLUSION

Quantitative analysis has been shown to be a useful adjunct in analyzing ^{201}Tl myocardial scans and will likely prove helpful with the newer technetium agents as well. It offers a means of standardization, thus eliminating inter-observer variations in interpretation. However, since potential artifacts may skew results, quantitative analysis should always be used in conjunction with visual interpretation. Although current computer methods rely on comparison of scans to a normal file, future program may be able to employ either neural networks or expert systems and thus improve accuracy by eliminating artifactual defects.

REFERENCES

1. Gabor FV, Christian PE, Datz FL, Gullberg GT, Morton KA. Computer-assisted diagnosis of pulmonary embolism on ventilation-perfusion lung imaging. (Work-in-Progress.) *J Nucl Med* 1991;32:1837.
2. DePasquale EE, Nody AC, DePuey EG, et al. Quantitative rotational thallium-201 tomography for identifying and localizing coronary artery disease. *Circulation* 1988;77:316–327.
3. Cedars-Sinai PTQ. *Nuclear Medical Imaging Systems Operator's Guide.* Bedford Heights, Ohio: Picker International Inc.; 1991.
4. DePuey EG, Garcia EV, Ezquerra NF. Three-dimensional techniques and artificial intelligence in T1-201 cardiac imaging. *AJR* 1989;152:1161–1168.
5. Eisner RL, Tamas MJ, Cloninger K, et al. Normal SPECT T1-201 bull's-eye display: gender differences. *J Nucl Med* 1988;29:1902–1909.
6. Rabinovitch M, Suissa S, Elstein J, et al. Sex-specific criteria for interpretation of T1-201 myocardial uptake and washout studies. *J Nucl Med* 1986;27:1837–1841.
7. DePuey EG, Garcia EV. Optimal specificity of T1-201 SPECT through recognition of imaging artifacts. *J Nucl Med* 1989;30:441–449.
8. Klein JL, Garcia EV, DePuey EG, et al. Reversibility bull's-eye: a new polar bull's-eye map to quantify reversibility of stress-induced SPECT thallium-201 myocardial perfusion defects. *J Nucl Med* 1990;31:1240–1246.
9. Garcia EV, DePuey EG, Sonnemaker RE, et al. Quantification of the reversibility of stress-induced T1-201 myocardial perfusion defects: a multicenter trial using bull's-eye polar maps and standard normal limits. *J Nucl Med* 1990;31:1761–1765.
10. VanTrain KF, Maddahi J, Berman DS, et al. Quantitative analysis of tomographic stress T1-201 myocardial scintigrams: a multicenter trial. *J Nucl Med* 1990;31:1168–1179.
11. Garcia EV, VanTrain K, Maddahi J, et al. Quantification of rotational T1-201 myocardial tomography. *J Nucl Med* 1985;26:17–26.
12. Eisner R, Churchwell A, Noever T, et al. Quantitative analysis of the tomographic T1-201 myocardial bullseye display: critical role of correcting for patient motion. *J Nucl Med* 1988;29:91–97.
13. Geckle WJ, Frank TL, Links JM, Becker LC. Correction for patient and organ movement in SPECT: application to exercise T1-201 cardiac imaging. *J Nucl Med* 1988;29:441–450.
14. Datz FL, Gullberg G, Gabor FV, Morton KA. SPECT myocardial perfusion imaging update. *Semin Ultrasound, CT, MR* 1991;12:28–44.
15. Mester J, Weller R, Clausen M, et al. Upward creep of the heart in exercise T1-201 single-photon emission tomography: clinical relevance and a simple correction method. *Eur. J. Nucl Med* 1991;18:184–190.
16. Plankey MW, Clark MW, Strickland MD. A T1-201 SPECT artifact associated with leg flexion: case report. *J Nucl Med Technol* 1991;19:31–32.
17. VanTrain KF, Berman DS, Garcia EV, et al. Quantitative analysis of stress thallium-201 myocardial scintigrams: a multicenter trial. *J Nucl Med* 1986;27:17–25.
18. Botvinick EH, O'Connell WJ, Dae MW, Hattner RS, Schechtmann NM. Analysis of T1-201 "washout" from parametric color-coded images. *J Nucl Med* 1988;29:302–310.
19. Wackers FJT, Fetterman RC, Mattera JA, Clements JP. Quantitative planar T1-201 stress scintigraphy: a critical evaluation of the method. *Semin Nucl Med* 1985;15:46–66.
20. Sigal SS, Soufer R, Fetterman PC, Mattera JA, Wackers FJT. Reproducibility of quantitative planar thallium-201 scintigraphy: quantitative criteria for reversibility of myocardial perfusion defects. *J Nucl Med* 1991;32:759–765.
21. Gai R, Port SC. Arm vein uptake of T1-201 during exercise: incidence and clinical significance. *J Nucl Med* 1986;27:1353–1357.
22. Kaul S, Chesler DA, Pohost GM, Strauss HE, Okada RD, Boucher CA. Influence of peak exercise heart rate on normal T1-201 myocardial clearance. *J Nucl Med* 1986;27:26–30.
23. Nordrehaug JE, Danielsen R, Vik-Mo H. Effects of heart rate on myocardial T1-201 uptake and clearance. *J Nucl Med* 1989;30:1972–1976.
24. Lancaster JL, Starling MR, Kopp DT, Lasher JC, Blumhardt R. Effect of errors in re-angulation on planar and tomographic T1-201 washout profile curves. *J Nucl Med* 1985;26:1445–1455.
25. Dilsizian V, Rocco TP, Freedman MT, Leon MB, Bonow RO. Enhanced detection of ischemic but viable myocardium by the re-injection of thallium after stress-redistribution imaging. *N Engl J Med* 1990;323:141–146.
26. Iskandrian AS, Hew J, Askenase A, Segal BL, Auerbach N. Dipyridamole cardiac imaging. *Am Heart J* 1988;115:432–443.
27. Kahn JK, McGhie I, Akers MS, et al. Quantitative rotational tomography with T1-201 and Tc-99m 2-methoxy-isobutyl-isonitrile: a direct comparison in normal individuals and patients with coronary artery disease. *Circulation* 1989;79:1282–1293.
28. Maddahi J, Kiat H, VanTrain KF, et al. Myocardial perfusion imaging with Tc-99m Sestamibi SPECT in the evaluation of coronary artery disease. *Am J Cardiol* 1990;66:55E–62E.
29. Boone JM, Sigillito VG, Shaber GS. Neural networks in radiology: an introduction and evaluation in a signal detection task. *Med Phys* 1990;17:234–241
30. Boone M, Gross GW, Greco-Hunt V. Neural networks in radiologic diagnosis: I. Introduction and illustration. *Investig Radiol* 1990;25:1012–1016.
31. Gross GW, Boone JM, Greco-Hunt V, Greenberg B. Neural networks in radiologic diagnosis: II. Interpretation of neonatal chest radiographs. *Investig Radiol* 1990; 25:1017–1023.
32. Shah R, Anderson J. Evaluation of simulated stress thallium data by back propagation neural network (BPNN) on personal computer. (Abstract.) *J Nucl Med* 1990;31:1580.
33. Wang DC, Karvelis KC. Computer interpretation of thallium SPECT studies based on neural network analysis. (Abstract.) *J Nucl Med* 1990;31:1582.